Interaction of 2'-Deoxyadenosine with cis-2-Butene-1,4-dial: Computational Approach to Analysis of Multistep Chemical Reactions

ARTICLE *in* THE JOURNAL OF PHYSICAL CHEMISTRY A · MARCH 2012

Impact Factor: 2.69 · DOI: 10.1021/jp211911u · Source: PubMed

4 AUTHORS, INCLUDING:

Dmytro Mykolayovych Hovorun
National Academy of Sciences of Ukraine
392 PUBLICATIONS **2,079** CITATIONS

THE JOURNAL OF PHYSICAL CHEMISTRY A

Article

pubs.acs.org/JPCA

Interaction of 2′-Deoxyadenosine with *cis*-2-Butene-1,4-dial: Computational Approach to Analysis of Multistep Chemical Reactions

Liudmyla Sviatenko,[†,‡] Leonid Gorb,[†,§,⊥] Dmytro Hovorun,[§,⊥] and Jerzy Leszczynski*[,†]

[†]Interdisciplinary Center for Nanotoxicity, Department of Chemistry and Biochemistry, Jackson State University, Jackson, Mississippi 39217, United States

[‡]Kirovohrad State Pedagogical University, Kirovohrad 25006, Ukraine

[§]Institute of Molecular Biology and Genetics and [⊥]State Key Laboratory in Molecular and Cell Biology, NAS of Ukraine, 150 Zabolotny Str., Kyiv 03143, Ukraine

Supporting Information

ABSTRACT: The computational analysis of multistep chemical interactions between 2′-deoxyadenosine and *cis*-2-butene-1,4-dial has been performed. The applied protocol includes generation of a multistep Gibbs free-energy reaction profile (PCM/M05-2X/6-311+G(d) level) for the transformations of the reagents to products, followed by evaluation of the rate constants, construction of the corresponding kinetic equations, and solving them. Such a procedure allows one to significantly extend the number of experimentally determined steps by addition of the ones computationally predicted. The primary products of the reaction are found to be four diastereomeric adducts characterized by virtually the same stability. The acid-catalyzed dehydration of these adducts leads to a more stable secondary product. Computational verification of UV and NMR spectra has also been performed. It has been revealed that simulated UV and NMR spectra of primary and secondary 2′-deoxyadenosine adducts of *cis*-2-butene-1,4-dial are in agreement with the experimental observations.

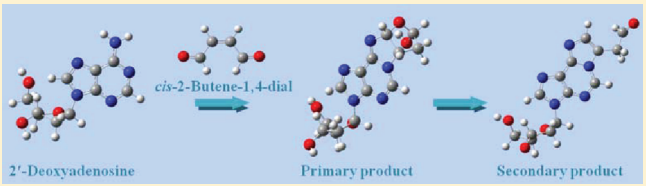

INTRODUCTION

It is well-known that the majority of real chemical processes could be represented as a number of elementary steps that define the reaction pathway. The most straightforward way to predict those pathways computationally is to apply ab initio[1] or classical reaction molecular dynamics.[2] However, in practice, such techniques, even with the aid of modern parallel high-performance algorithms and computers, permit consideration of only the transformation of chemical species at a quite high temperature.[3] In this paper, we present rather semiempirical way that allows efficient evaluation of those pathways. It is based on the application of static quantum chemical approximations and the limited information obtained from preliminary performed experimental studies of the multistep reaction. This approach also uses the information obtained from the experiment at the final step of our study, evaluation of the kinetics. It will be revealed that the suggested computational strategy allows one to go beyond the data obtained experimentally. The presented study applies the analysis of multistep chemical reactions described below to the interaction of *cis*-2-butene-1,4-dial (BDA) with 2′-deoxyadenosine (dAdo).

BDA represents a microsomal metabolite of furan,[4] an industrially important chemical found in cigarette smoke, air pollution, and sometimes canned or jarred foods that undergo heat treatment. It has been classified as a possible human carcinogen (group 2B).[5] This electrophile is also produced by oxidation of the 5′-position of 2′-deoxyribose in DNA.[6] Like other unsaturated aldehydes, BDA readily reacts with nucleophilic sites in biomolecules.[7−11] There is some evidence that BDA is an important genotoxic intermediate in furan-induced carcinogenesis (Scheme 1). It is mutagenic in the Ames assay[12] and causes DNA single-strand breaks and DNA cross-links in Chinese hamster ovary cells.[13]

There are just a few experimental studies of BDA reaction with DNA and nucleosides.[8−11,14,15] BDA reacts with 2′-deoxycytidine to form relatively stable primary oxadiazabicyclooctaimine adducts[8] and with 2′-deoxyguanosine and dAdo to form initial adducts that readily rearrange by dehydration to form substituted etheno adducts.[9] These adducts were observed in DNA isolated from *S. typhimurium* TA104 bacteria treated with mutagenic concentrations of BDA.[10] The correlation between the formation of BDA-derived DNA adducts and the mutagenicity in the Ames assay suggests that the formation of these adducts is responsible for the mutagenicity of BDA. The presence of low levels of the adducts in untreated DNA suggests that these adducts could be formed through an endogenous pathway. Therefore, this class of nucleoside adducts may have general importance in the mutagenesis and

Received: December 11, 2011
Revised: February 3, 2012
Published: February 8, 2012

Scheme 1

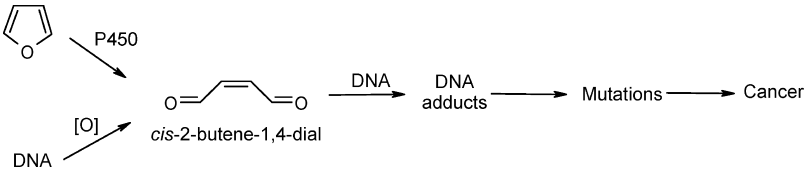

Scheme 2

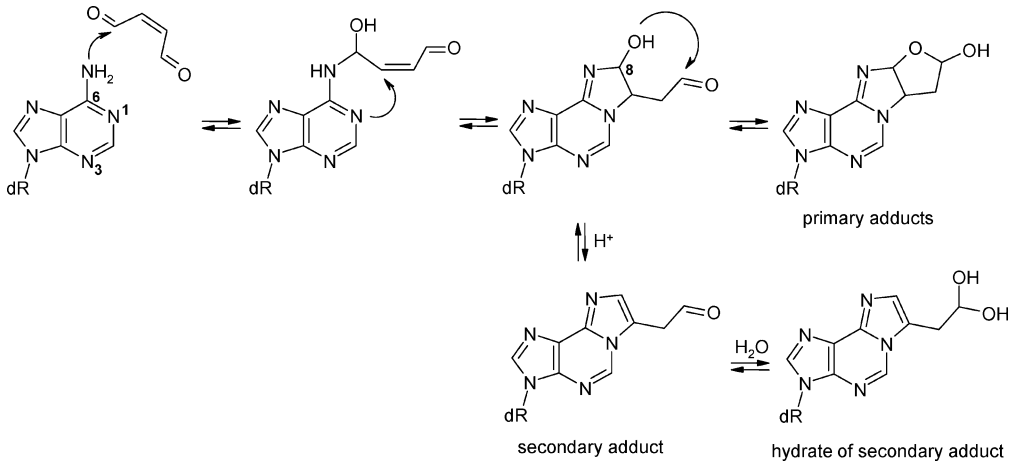

carcinogenesis associated with furan metabolism and oxidative DNA damage.

The present study focuses on interaction of BDA with dAdo.[16] Combination of UV absorbance, fluorescence, NMR, and mass spectral analysis[8,9,11] allows identification of the primary and secondary reaction products, which are diastereomeric hemiacetal forms of 3-(2′-deoxy-β-D-erythropentafuranosyl)-3,5,6,7-tetrahydro-6-hydroxy-7-(ethane-2″-al)-9*H*-imidazo-[1,2-α]purine-9-one and 1″-[3-(2′-deoxy-β-D-erythropentafuranosyl)-3H-imidazo[2,1-i]purin-8-yl]ethane-2″-al, respectively.[9,11] Consistent with those observations is a reaction mechanism[9] involving initial reaction of the C_1 atom of BDA with the exocyclic nitrogen atom N_6 of dAdo (Scheme 2). This event is followed by 1,4-addition of the adjacent endocyclic nitrogen atom N_1 to the double bond of the remaining α,β-unsaturated aldehyde and subsequent attack of the alcohol on the second aldehyde group to form the primary adducts. The incubation of the primary dAdo adducts at 37 °C resulted in the formation of a secondary product.[11] Because the half lives of the primary dAdo products at physiological pH are on the order of a few hours,[9] persistent adducts most likely exist as the rearrangement products. The ring-opened form of the primary adduct undergoes protonation at C_8−OH, causing dehydration to the secondary product, which is in equilibrium with its hydrate.[11] This product may induce point mutations and can also be expected to generate DNA−DNA and/or DNA−protein cross-links through the reactive aldehyde functionality.

Experimental studies of the interaction between dAdo and BDA[8−11,14,15] suggest only key intermediate products that characterize the interaction pathway (see Scheme 2). As we mentioned above, the transformation from one compound presented in Scheme 2 to another one is as usually a multistep process that is characterized by the presence of numerous intermediates, located as minima of the potential energy surfaces. Those minima are separated by maxima that govern the activation energy of the step (potential energy surface) or the activation Gibbs free energy (Gibbs free energy). The information on the values of activation energies are completely absent in experimental studies. Therefore, the aim of the presented investigation is, to a large extent, to augment the information that has been obtained experimentally. To accomplish this goal, we have chosen the M05-2X version[17] of density functional theory approximation,[18] which has been specially designed to reproduce the thermodynamics and kinetics of chemical reactions with accuracy close to that experimentally observed.

■ COMPUTATIONAL METHODOLOGY

All calculations were performed with the Gaussian 09 program package.[19] The relevant stationary points (reagents, intermediates, transition states, and products) were fully optimized at the M05-2X/6-311+G(d) level.[17] A selected water molecule was used as a catalyst when it was necessary. Single-point calculations in aqueous solution were carried out at the gas-phase-optimized geometry for the adducts and corresponding transition states using PCM at the M05-2X/6-311+G(d) level of theory. The relevant stationary points (reagents, intermediates, transition states, and products) were fully optimized at the PCM/M05-2X/6-311+G(d) level in the case of the acid-catalyzed mechanism. All stationary points were further characterized as minima with all real frequencies or as transition states with the only one imaginary frequency by computations of analytic harmonic vibrational frequencies at the same theory level as the geometry optimization.

We also would like to highlight that because there has been no any evidence in the literature on the participation of the enzymes in considered transformations, we also did not consider such possibilities. However, we did not exclude that some of the steps are catalyzed by enzymes that are not yet determined.

UV and vis spectra of initial compounds and products were simulated at the PCM/M05-2X/6-311+G(d) level. NMR

dx.doi.org/10.1021/jp211911u | J. Phys. Chem. A 2012, 116, 2333−2342

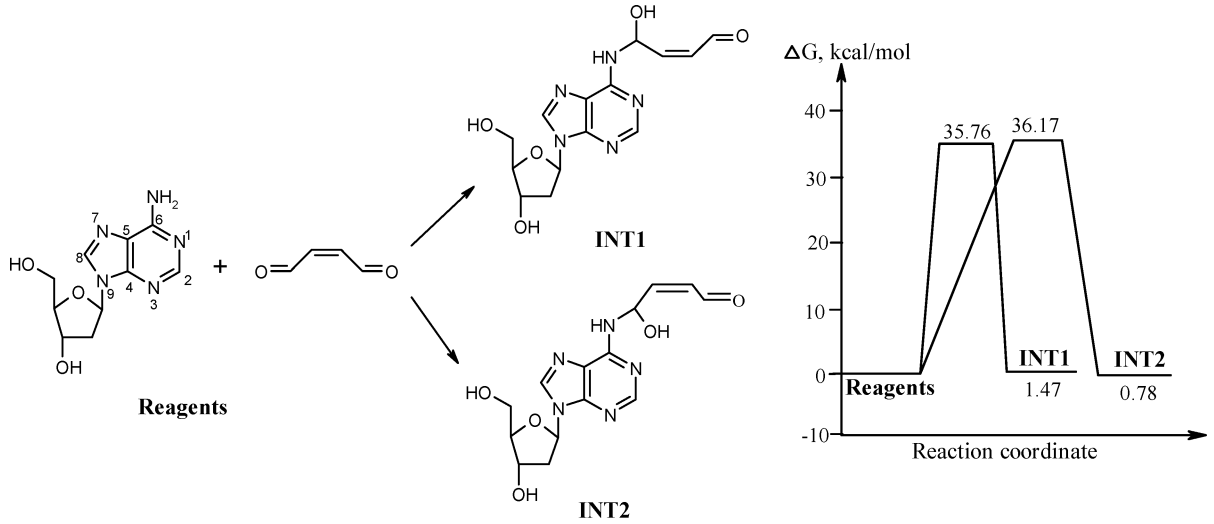

Figure 1. PCM/M05-2X/6-311+G(d)//M05-2X/6-311+G(d) computer-generated initial pathways of dAdo reaction with BDA and the corresponding Gibbs free-energy diagram.

spectra of products were calculated by applying the M05-2X method that uses the gauge-independent atomic orbital (GIAO) NMR computational formalism and PCM solvation model.

Uni- and bimolecular rate constants were calculated according to the following equations

$$k_{\text{uni}} = \frac{k \cdot T}{h} \cdot e^{-\Delta G_T^{\ddagger}/RT} \ (s^{-1}) \tag{1}$$

$$k_{\text{bi}} = \frac{k \cdot T}{h} \cdot e^{-\Delta G_T^{\ddagger}/RT} \cdot \left(\frac{1}{c}\right) \ (L \cdot mol^{-1} \cdot s^{-1}) \tag{2}$$

where k is the Boltzmann constant, T is temperature, h is Planck's constant, $\Delta G_T^{\ddagger}$ is Gibbs free energy, R is the universal gas constant, and c is a transformation coefficient equal to 1 $mol \cdot L^{-1}$.

The rate constants k_{uni} and k_{bi} calculated using eqs 1 and 2 were applied to predict the rate of reagent decay and the rate of accumulation of products and intermediates that are presented in Scheme 2. For this purpose, the system of differential equations having the following general form (the real form of the differential equations is presented in the Supporting Information) has been solved

$$\sum_i \frac{dn_i}{dt} = \sum_{j(j\neq i)} k_{ji} n_j - n_i \sum_{l(l\neq i)} k_{il}$$

$$\sum_i \frac{dn_i}{dt} = \sum_{j(j,m\neq i)} k_{ji} n_j n_m - n_i \sum_{l(l,o\neq i)} k_{il} n_o \tag{3}$$

The systems of kinetic in eqs 3 were solved by using a Mathcad 15 program. The initial concentrations of dAdo and BDA (corresponding to experimental data) were equal to 5 and 25 mmol/L, respectively, and the temperature was 37 °C.

RESULTS AND DISCUSSION

Before discussing the possible pathways of transformation, we would like to verify computationally available experimental data obtained with the aid of UV−vis and NMR spectroscopy. We will provide here only the most essential data of those simulations. Other details are included in the Supporting Information.

We have found that the predicted UV spectra of dAdo and dAdo adducts of BDA are quite similar to their experimental spectra[9,11] (see Figure S1 of the Supporting Information). Primary adducts have also identical UV spectra with λ_{max} at 237 nm and a slight shoulder at 247 nm (exptl 263 and 275 nm). The UV spectrum of the secondary product has absorption maxima at 215 and 270 nm (exptl 231 (high absorbance), 269, 279, and 302 nm (low absorbance)).

Calculated ^{13}C NMR spectra for primary dAdo adducts of BDA in water reveal clear similarity to experimental data. The largest difference between calculated and experimental ^{13}C chemical shifts does not exceed 13 ppm. The calculated ^{1}H chemical shifts for primary and secondary dAdo adducts of BDA in water are also in good correspondence with experimental data (other details and comments on the comparison of experimental and computationally designed NMR data may be found by analyzing the data of Tables S1−S2 and reading the comments in the Supporting Information).

Because all computationally generated spectra are in good (or excellent) correspondence with the ones experimentally observed, we conclude that the geometrical structure of the species considered above has been verified and computationally confirmed.

Reaction Mechanism of Primary dAdo Adducts of BDA Formation. Computational simulation on an initial attack of the exocyclic N_6 atom of dAdo onto the carbonyl atom of BDA reveals that such a process leads to two possible stereoisomers with similar stability (**INT1** and **INT2**) (Figure 1). The obtained data suggest that the formation of the C−N bond and proton transfer between reactants occurs in one step. The formation and breakage of the C−N and C−O bonds are predicted to take place before the proton transfers between heteroatoms.

Further transformation of **INT1** and **INT2** intermediates occurs in the direction of five-membered cycle formation. Direct intermolecular attack of the endocyclic N_1 atom on the ethene carbon atom in **INT1** can yield two possible stereomeric intermediates, **INT4** and **INT7** (Figure 2). The Gibbs free-energy activation barriers for these pathways are 16.61 and 18.51 kcal/mol, respectively. These zwitterionic intermediates

dx.doi.org/10.1021/jp211911u | J. Phys. Chem. A 2012, 116, 2333−2342

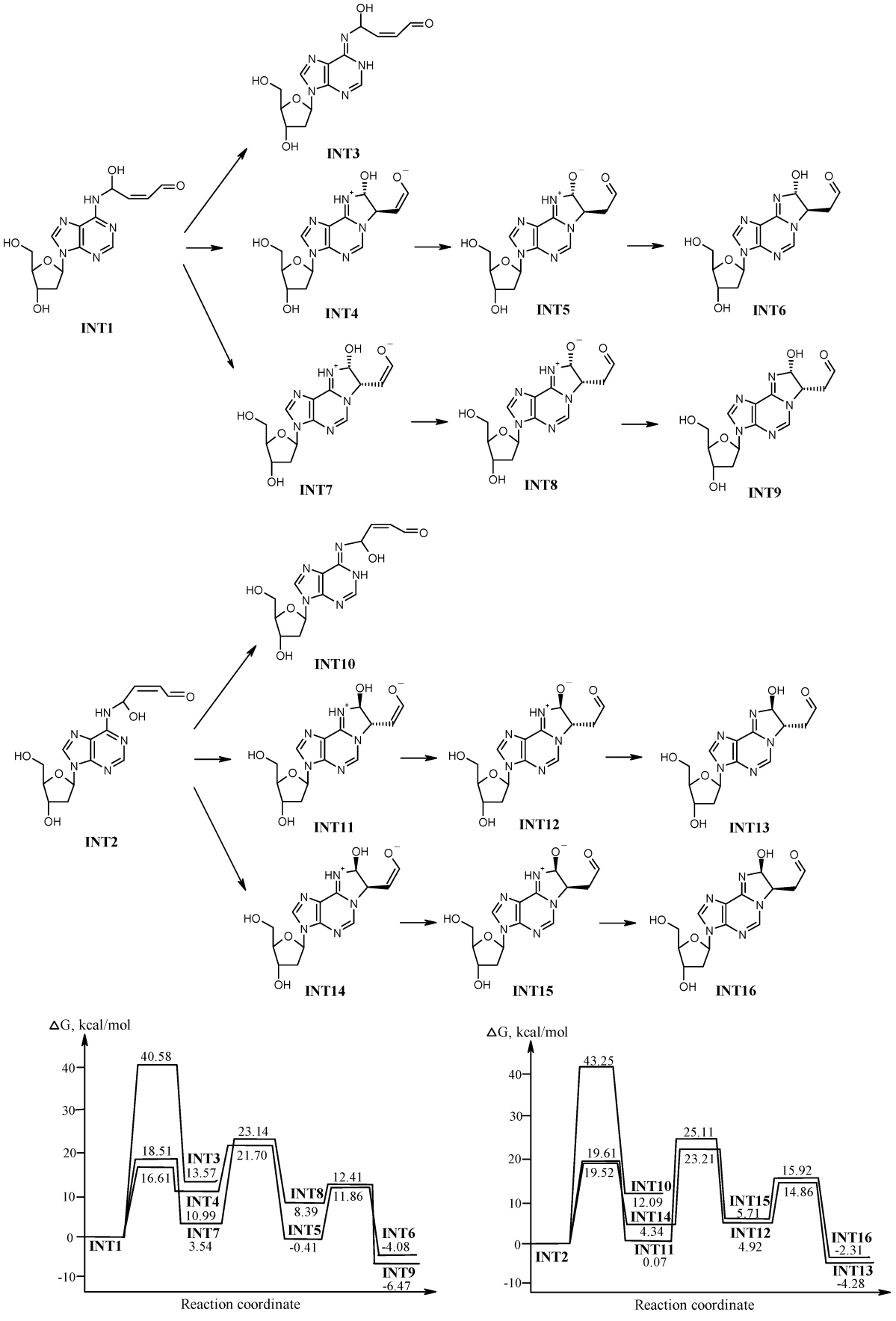

Figure 2. PCM/M05-2X/6-311+G(d)//M05-2X/6-311+G(d) computer-generated pathways of **INT1** and **INT2** transformations and the corresponding Gibbs free-energy diagrams.

dx.doi.org/10.1021/jp211911u | *J. Phys. Chem. A* 2012, 116, 2333−2342

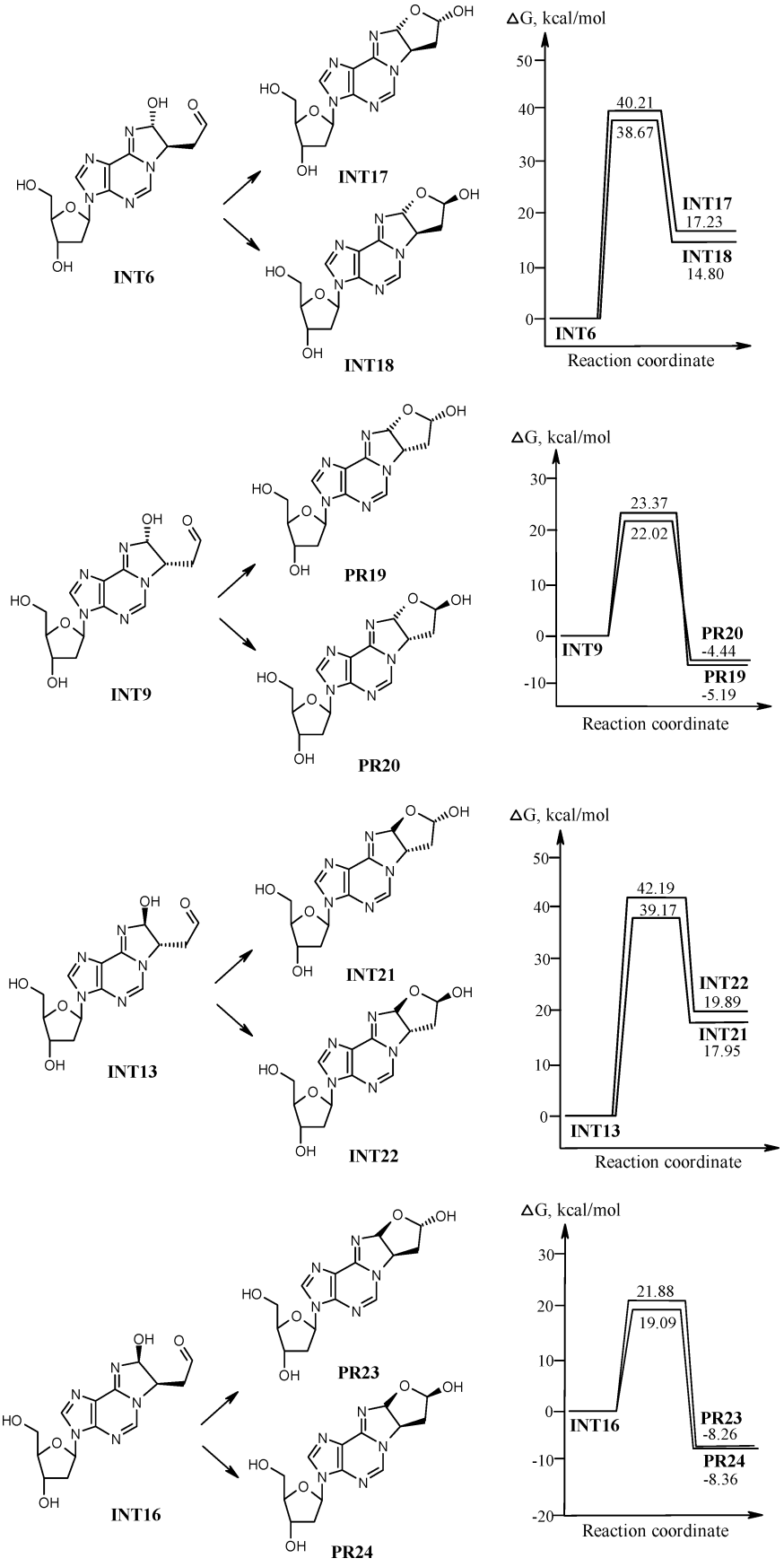

Figure 3. PCM/M05-2X/6-311+G(d)//M05-2X/6-311+G(d) computer-generated pathways of **INT6**, **INT9**, **INT13**, and **INT16** transformations and the corresponding Gibbs free-energy diagrams.

dx.doi.org/10.1021/jp211911u | *J. Phys. Chem. A* 2012, 116, 2333−2342

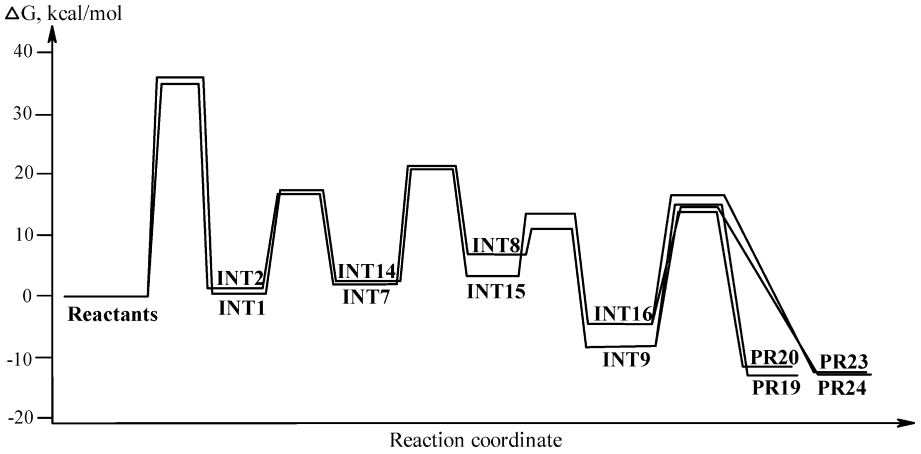

Figure 4. Relative Gibbs free-energy profiles (kcal/mol) for the most favorable pathways of the primary dAdo adducts of BDA formation calculated at the PCM/M05-2X/6-311+G(d)//M05−2X/6-311+G(d) level.

transform to more stable **INT6** and **INT9** by double proton transfer between oxygen and carbon atoms and between nitrogen and oxygen atoms. The cycle closing for **INT2** produces two stereoisomeric intermediates **INT11** and **INT14**, which are subsequently exposed by two-step rearrangement into **INT13** and **INT16.** The Gibbs free activation energies for these stages do not exceed 26 kcal/mol. Therefore, transformation of **INT1** and **INT2** proceeds through a set of zwitterionic intermediates and results in formation of four isomeric intermediates (**INT6**, **INT9**, **INT13**, **INT16**) (Figure 2). Preliminary intermolecular hydrogen transfer between nitrogen atoms in **INT1** and **INT2** with formation of **INT3** and **INT10**, respectively, is not realized because of high Gibbs free activation energy (40.58 and 43.25 kcal/mol, respectively).

The nucleophilic attack of the hydroxyl group on the carbonyl carbon in **INT9** and **INT16** intermediates causes cyclization with formation of a five-membered ring and is accompanied by proton transfer between oxygen atoms, leading to **PR19** and **PR20** products and products **PR23** and **PR24**, respectively (Figure 3). These cyclizations require activation Gibbs free energies of 19−24 kcal/mol. The four diastereomeric products have the same stability and differ by the orientation of the five-membered furan cycle and the hydroxyl group. The nucleophilic attack of the hydroxyl group on the carbonyl carbon in **INT6** and **INT13** intermediates is not possible because of steric separation of these functional groups. This is suggested by high activation Gibbs free energies of 38−42 kcal/mol for these pathways (Figure 3).

On the basis of the obtained results, one may conclude that the formation of primary dAdo adducts of BDA can be described as a consecutive five-step reaction that has the rate determined by the very first step (see Figure 1).

Summarizing, Figure 4 presents the general profile of the change of the Gibbs free energy along the reaction coordinate that starts from the reactants and ends at the primary products.

The DFT M05-2X functional belongs to the family of functionals that is designed to quantitatively describe the thermochemical properties, including chemical kinetics.[17] Therefore, the values of the Gibbs free-energy barriers presented in Figures 1−3 have been converted to the set of rate constants. Those rate constants are used to develop computer-generated kinetics for reactants, products, and intermediates. Such rate constants are presented in the Supporting Information in the Table S3 along with the kinetic equations (Scheme S1) that describe the chemical process displayed in Figures 1−3.

Because the kinetics of the reagents decay and the accumulation of the products is already experimentally studied and published,[9] one could compare the experimental and in silico results. Such a comparison reveals that in silico kinetics predicts the rate of chemical reactions presented in Figures 1−3 to be significantly slower than the experimentally observed rate. Actually, the absence of quantitative correspondence is expected due to the rather simple continuum approximation applied here to model the influence of water bulk. In our opinion, this is the main source of the inaccuracy. The analysis of the data in the literature suggests that inclusion of a larger amount of explicit water molecules, involved in hydration of transition states, leads to their stabilization and the decrease of the activation Gibbs free energy.[20] However, application of a single scaling factor, which results in a 33% decrease of all activation energies presented in Figures 1−3, makes the observed and computationally predicted kinetics virtually the same as the experimental one (see Figure 5) both for the decay

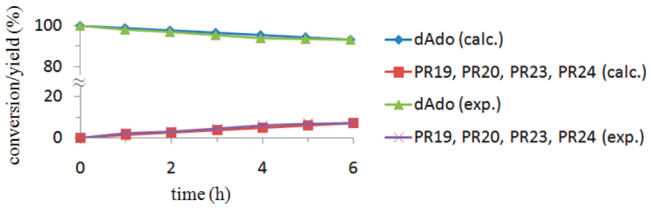

Figure 5. Kinetic plot of the primary dAdo adducts of the BDA (PR19, PR20, PR23, PR24) formation reaction calculated at 37 °C at the PCM/M05-2X/6-311+G(d)//M05-2X/6-311+G(d) level.

of reagents and accumulation of products. Therefore, our next step of discussion will be based on the application of those adjusted rate constants.

We also understand that the correspondence of computationally generated and experimentally observed data presented in Figure 5 does not guarantee that the pathway displayed in Figures 1−4 is the one that is detected experimentally. Nevertheless, we would like to highlight that in contrast to experimental data, we calculated a full set of the rate constants. This allowed us to analyze the kinetics of any step of the multistep chemical reaction. By applying such an analysis to the set of chemical transformations presented in Figures 1−4, one

dx.doi.org/10.1021/jp211911u | J. Phys. Chem. A 2012, 116, 2333−2342

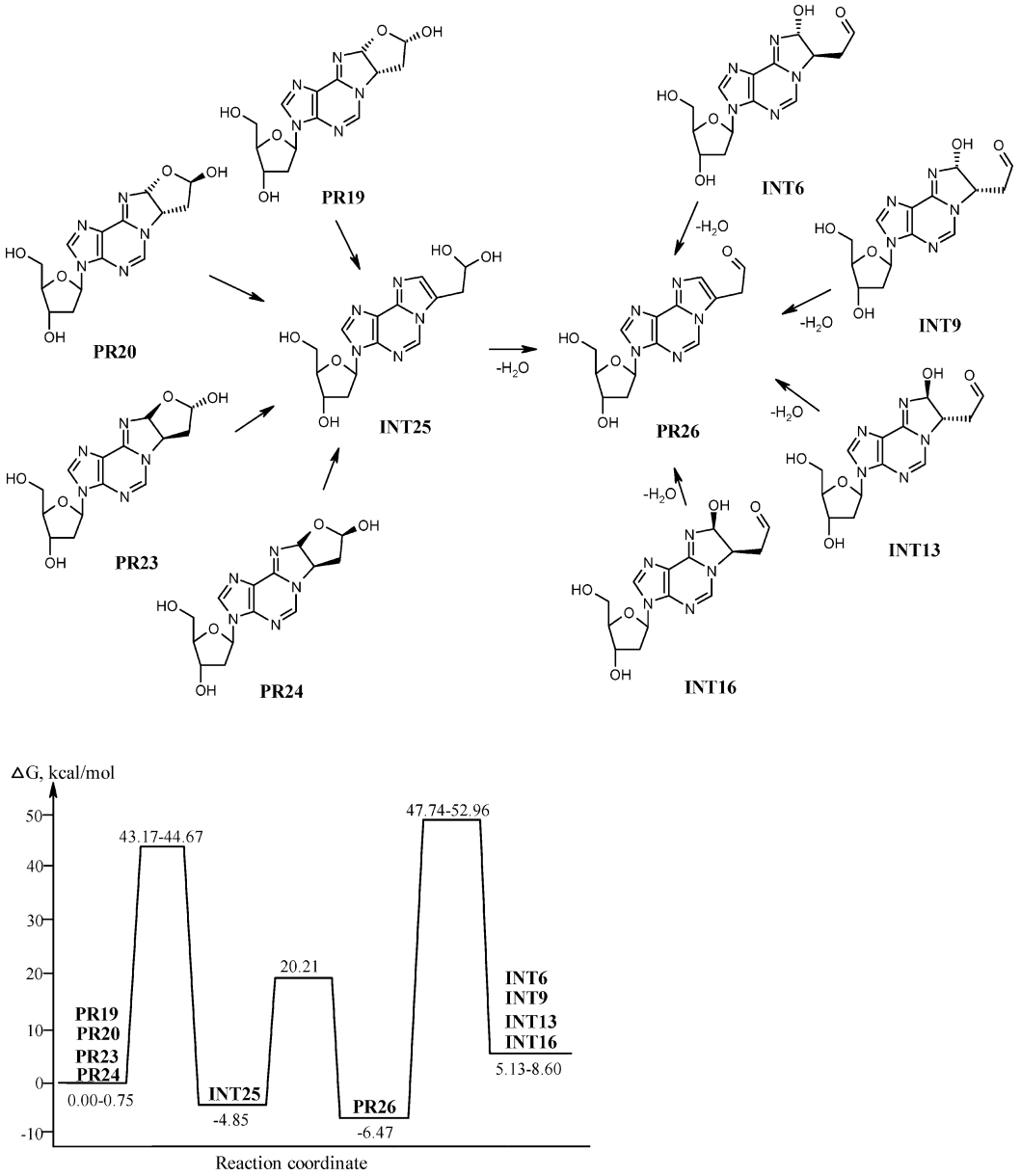

Figure 6. PCM/M05-2X/6-311+G(d)//M05-2X/6-311+G(d) computer-generated pathways of primary → secondary product transformation and the corresponding Gibbs free-energy diagram.

can conclude that though such intermediates as **INT5**, **INT6**, **INT9**, and so forth have relative Gibbs free energies comparable to the free energy of the reagents, they cannot be observed experimentally due to very low abundance during the investigated reaction timing (see Figure S3, Supporting Information).

Reaction Mechanism of Primary → Secondary Diastereomeric Adduct Transformation. As we already mentioned above, the incubation of initial diastereomeric reaction products of BDA and dAdo at 37 °C resulted in the formation of a secondary product.[11] This process may occur in two ways. The first way represents furan cycle opening followed by water molecule abstraction. The second one proceeds through reversion of primary products to their open forms (**INT6**, **INT9**, **INT13**, **INT16**) and subsequent dehydration. We found that both of these directions require more than 40 kcal/mol of activation free energy (Figure 6). Therefore, they are rather not feasible. The experimental data show that a minimum of the half lives for primary adducts was observed between pH 6 and 7. Therefore, we have considered an acid-catalyzed mechanism for primary → secondary adduct transformation. This mechanism was modeled on primary products **PR19**, **PR20**, **PR23**, and **PR24** using an acetic acid molecule as a protonating agent (Figure 7). The addition of a proton to an open form of the primary products **INT9** and **INT16** occurs on the nitrogen atom and leads to positively charged intermediates **INT27** and **INT28**. The proton transfer from the nitrogen atom to the hydroxyl group causes **INT27** and **INT28** to lose a water molecule and form intermediates **INT29** and **INT30**, respectively. The proton abstraction from **INT29** and **INT30** yields secondary product **PR26**.

We concluded that acid-catalyzed dehydration appears to be more realistic compared to the water-catalyzed mechanism, in agreement with experimental data.[11] As before, the obtained relative Gibbs free-energy profile presented in Figure 7 has been converted to kinetic equations displayed in Scheme S2

dx.doi.org/10.1021/jp211911u | J. Phys. Chem. A 2012, 116, 2333−2342

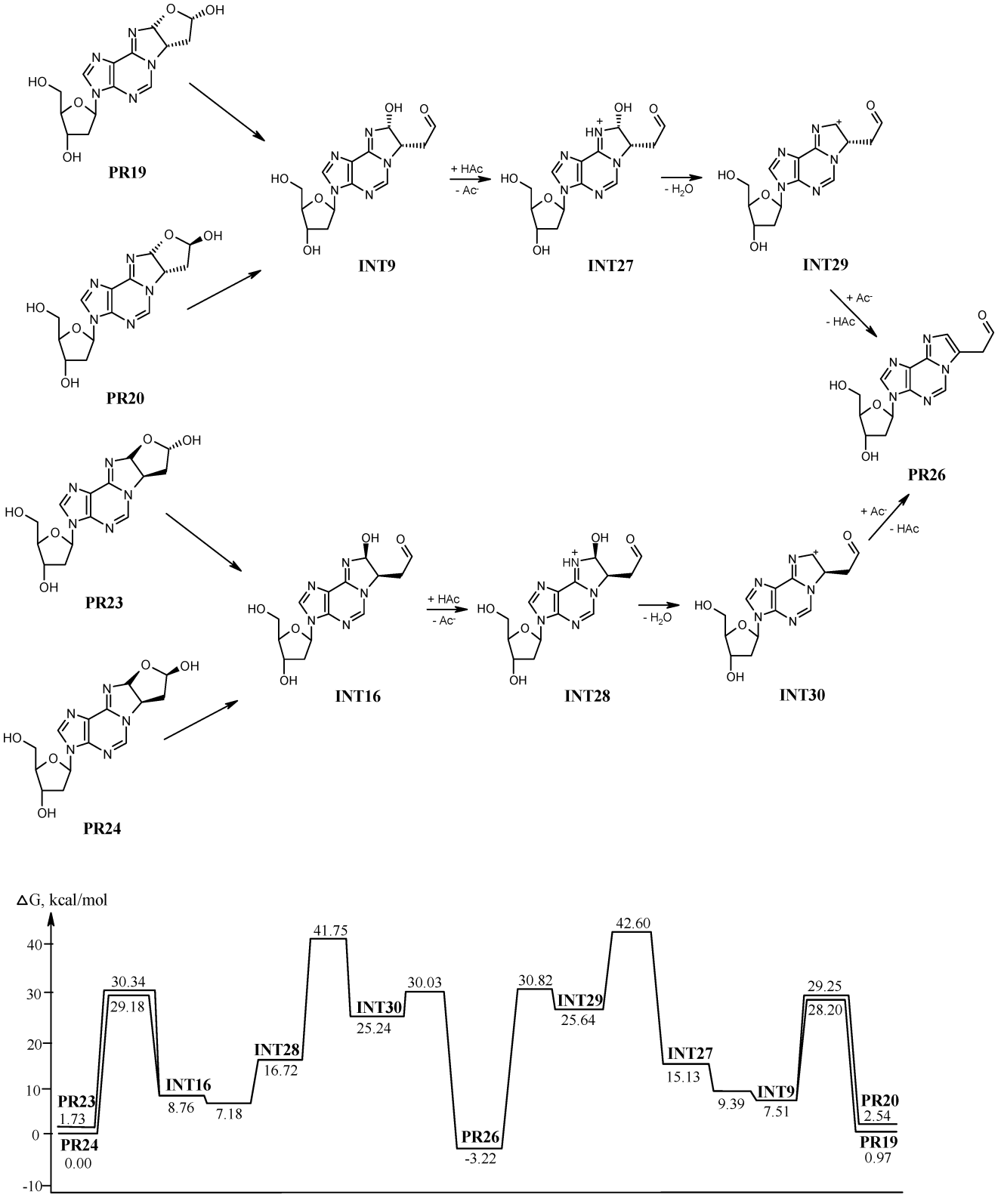

Figure 7. PCM/M05-2X/6-311+G(d) computer-generated pathways of acid-catalyzed primary → secondary adduct transformation and the corresponding Gibbs free-energy diagram.

and Table S4 of the Supporting Information. According to the experimental data,[11] the half life transformation for the primary to secondary diastereomeric adducts is estimated to be less than 2 h. Decreasing the Gibbs free-energy barriers by 44% (application of a single scaling factor) allows one to obtain good agreement of the reaction half times between the calculated (1.14 h) and the experimental values. The computationally predicted kinetic plots of products and intermediates are shown in Figures 8 and S3 (Supporting Information), respectively.

dx.doi.org/10.1021/jp211911u | J. Phys. Chem. A 2012, 116, 2333−2342

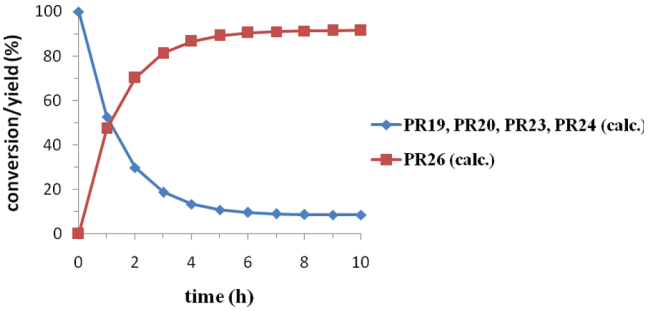

Figure 8. Kinetic plot for the primary → secondary dAdo adducts of the BDA transformation reaction calculated at 37 °C at the PCM/M05-2X/6-311+G(d) level.

Applying kinetic analysis to the set of chemical transformations presented in Figure 7, one can conclude (similarly to the previous conclusions regarding the intermediates of primary reactions) that such intermediates as **INT9**, **INT16**, **INT29**, and **INT30** that have much higher relative Gibbs free energies compared with the free energy of the reagents cannot be observed experimentally due to very low abundance during the investigated reaction timing (see Figure S3, Supporting Information).

CONCLUSIONS

This work presents the results of the quantum chemical investigation of a multistep chemical interaction between dAdo and BDA. The computational protocol for such an analysis includes quantum chemical generation of a multistep Gibbs free-energy reaction profile for the transformations of the reagents to products, evaluation of the rate constants, construction of the corresponding kinetic equations, and solving them. Such a procedure allows one to significantly extend the number of experimentally determined steps by augmenting them by ones predicted computationally.

The suggested reaction pathways along with the simulated UV and NMR spectra indicate that the primary and secondary dAdo reaction products represent hemiacetal forms of 3-(2′-deoxy-β-D-erythropentafuranosyl)-3,5,6,7-tetrahydro-6-hydroxy-7-(ethane-2″-al)-9*H*-imidazo[1,2-α]purine-9-one (**PR19**, **PR20**, **PR23**, **PR24**) and 1″-[3-(2′-deoxy-β-D-erythropentafuranosyl)-3*H*-imidazo[2,1-i]purin-8-yl]ethane-2″-al (**PR26**), respectively, which is in agreement with the experimental results.

On the basis of the predicted pathways, the kinetic models for the formation of primary and secondary products have been developed. It has been found that the formation of primary dAdo adducts of BDA can be described as a consequent five-step process, which involves the initial reaction of the exocyclic nitrogen atom N_6 of dAdo with the C_1 atom of BDA, further addition of the adjacent endocyclic nitrogen atom N_1 of dAdo to the double bond of the remaining α,β-unsaturated aldehyde, and final attack of the hydroxyl on the second aldehyde group. Four-step transformation of the primary products to a secondary adduct follows through the cycle opening and the acid-catalyzed dehydration.

The obtained results demonstrate that under mild, biological conditions, BDA reacts with dAdo to form a stable adduct that could be responsible for its mutagenesis. We believe that our study reveals and explains a general mechanism that characterizes interactions of dAdo with other α,β-unsaturated aldehydes.

ASSOCIATED CONTENT

Supporting Information

The UV spectra for dAdo and primary and secondary dAdo adducts of BDA PCM/M05-2X/6-311+G(d) calculated UV spectra (a) and (b) experimental UV spectra from ref 11 (Figure S1); the numbering of primary and hydrated secondary dAdo adducts of BDA (Figure S2); the PCM/M05-2X/6-311+G(d) calculated ^{13}C NMR spectra for primary dAdo adducts of BDA in water (Table S1); the PCM/M05-2X/6-311+G(d) calculated ^{1}H NMR spectra for primary and hydrated secondary dAdo adducts of BDA in water (Table S2); the system of differential equations for the kinetic model of primary adduct formation (Scheme S1); the PCM/M05-2X/6-311+G(d)//M05-2X/6-311+G(d) calculated Gibbs free energies (kcal/mol) and rate constants (s^{-1}, $L{\cdot}mol^{-1}{\cdot}s^{-1}$) for the kinetic model of primary adduct formation (Table S3); the system of differential equations for the kinetic model of primary → secondary adduct transformation (Scheme S2); the PCM/M05-2X/6-311+G(d) calculated Gibbs free energies (kcal/mol) and rate constants (s^{-1}) for the kinetic model of primary → secondary adduct transformation (Table S4); and the plots of the concentration versus time for intermediates calculated at 37 °C at the PCM/M05-2X/6-311+G(d)//M05-2X/6-311+G(d) level (Figure S3). This material is available free of charge via the Internet at http://pubs.acs.org.

AUTHOR INFORMATION

Corresponding Author

*Address: Interdisciplinary Center for Nanotoxicity, Department of Chemistry and Biochemistry, Jackson State University, 1325 J.R. Lynch Street, P.O. Box 17910, Jackson, MS 39217-0510, U.S.A. Tel: 601-979-3482. Fax: 601-979-7823. E-mail: jerzy@icnanotox.org.

Notes

The authors declare no competing financial interest.

ACKNOWLEDGMENTS

This work has been supported by the NSF CREST Interdisciplinary Center for Nanotoxicity, Grant # HRD-0833178. The computation time was provided by the Extreme Science and Engineering Discovery Environment (XSEDE) by National Science Foundation Grant Number OCI-1053575 and XSEDE award allocation Number DMR110088 and by the Mississippi Centre for Supercomputer Research.

REFERENCES

(1) Marx, D.; Hutter, J. *Ab Initio Molecular Dynamics: Basic Theory and Advanced Methods*; Cambrige University Press: Cambrige, U.K., 2009.

(2) van Duin, A. C. T.; Dasgupta, S.; Lorant, F.; Goddard, W. A. III. *J. Phys. Chem. A* **2001**, *105*, 9396−9409.

(3) (a) Isayev, O.; Gorb, L.; Qasim, M.; Leszczynski, J. *J. Phys. Chem. B* **2008**, *112*, 11005−11013. (b) Zhang, L.; Zybin, S.; van Duin, A. C. T.; Dasgupta, S.; Goddard, W. A.; Kober, E. J. *J. Phys. Chem. A* **2009**, *113*, 10619−10640.

(4) Chen, L.-J.; Hecht, S. S.; Peterson, L. *Chem. Res. Toxicol.* **1995**, *8*, 903−906.

(5) (a) National Toxicology Program. *9th Report on Carcinogens*; U.S. Department of Health and Human Services: Washington, DC, 2000. (b) National Toxicology Program. *11th Report on Carcinogens*; U.S. Department of Health and Human Services: Washington, DC, 2005. (c) U.S. Food and Drug Administration *Fed. Regist.* **2004**, *69*, 25911−25913.

(6) Chen, B.; Bohnert, T.; Zhou, X.; Dedon, P. C. *Chem. Res. Toxicol.* **2004**, *17*, 1406−1413.
(7) (a) Lu, D.; Peterson, L. A. *Chem. Res. Toxicol.* **2010**, *23*, 142−151. (b) Lu, D.; Sullivan, M. M.; Phillips, M. B.; Peterson, L. A. *Chem. Res. Toxicol.* **2009**, *22*, 997−1007. (c) Peterson, L. A.; Cummings, M. E.; Vu, C. C.; Matter, B. A. *Drug Metab. Dispos.* **2005**, *33*, 1453−1458. (d) Chen, L. J.; Hecht, S. S.; Peterson, L. A. *Chem. Res. Toxicol.* **1997**, *10*, 866−874.
(8) Gingipalli, L.; Dedon, P. C. *J. Am. Chem. Soc.* **2001**, *123*, 2664−2665.
(9) Byrns, M. C.; Predecki, D. P.; Peterson, L. A. *Chem. Res. Toxicol.* **2002**, *15*, 373−379.
(10) Byrns, M. C.; Vu, C. C.; Neidigh, J. W.; Abad, J.-L.; Jones, R. A.; Peterson, L. A. *Chem. Res. Toxicol.* **2006**, *19*, 414−420.
(11) Byrns, M. C.; Vu, C. C.; Peterson, L. A. *Chem. Res. Toxicol.* **2004**, *17*, 1607−1613.
(12) Peterson, L. A.; Naruko, K. C.; Predecki, D. *Chem. Res. Toxicol.* **2000**, *13*, 531−534.
(13) Marinari, U. M.; Ferro, M.; Sciaba, L.; Finollo, R.; Bassi, A. M.; Brambilla, G. *Cell Biochem. Funct.* **1984**, *2*, 243−248.
(14) (a) Rindgen, D.; Lee, S. H.; Nakajima, M.; Blair, I. A. *Chem. Res. Toxicol.* **2000**, *13*, 846−852. (b) Lee, S. H.; Rindgen, D.; Bible, R. H.; Hajdu, E.; Blair, I. A. *Chem. Res. Toxicol.* **2000**, *13*, 565−574.
(15) (a) Carvalho, V. M.; Di Mascio, P.; de Arruda Campos, I. P.; Douki, T.; Cadet, J.; Medeiros, M. H. G. *Chem. Res. Toxicol.* **1998**, *11*, 1042−1047. (b) Chaudhary, A. K.; Reddy, R. G.; Blair, I. A.; Marnett, L. J. *Carcinogenesis* **1996**, *17*, 1167−1170.
(16) (a) Zhurakivsky, R. O.; Hovorun, D. M. *Biopolym. Cell* **2007**, *23*, 45−53. (b) Zhurakivsky, R. O.; Hovorun, D. M. *Biopolym. Cell* **2007**, *23*, 363−368.
(17) (a) Zhao, Y.; Schultz, N. E.; Truhlar, D. G. *J. Chem. Theory Comput.* **2006**, *2*, 364. (b) Zhao, Y.; Truhlar, D. G. *Acc. Chem. Res.* **2008**, *41*, 157.
(18) Parr, R. G.; Yang, W. *Density-functional theory of atoms and molecules*; Oxford University Press: New York, 1989.
(19) Frisch, M. J.; Trucks, G. W.; Schlegel, H. B.; Scuseria, G. E.; Robb, M. A.; Cheeseman, J. R.; Scalmani, G.; Barone, V.; Mennucci, B.; Petersson, G. A.; Nakatsuji, H.; Caricato, M.; Li, X.; Hratchian, H. P.; Izmaylov, A. F.; Bloino, J.; Zheng, G.; Sonnenberg, J. L.; Hada, M.; Ehara, M.; Toyota, K.; Fukuda, R.; Hasegawa, J.; Ishida, M.; Nakajima, T.; Honda, Y.; Kitao, O.; Nakai, H.; Vreven, T.; Montgomery, J. A., Jr.; Peralta, J. E.; Ogliaro, F.; Bearpark, M.; Heyd, J. J.; Brothers, E.; Kudin, K. N.; Staroverov, V. N.; Kobayashi, R.; Normand, J.; Raghavachari, K.; Rendell, A.; Burant, J. C.; Iyengar, S. S.; Tomasi, J.; Cossi, M.; Rega, N.; Millam, J. M.; Klene, M.; Knox, J. E.; Cross, J. B.; Bakken, V.; Adamo, C.; Jaramillo, J.; Gomperts, R.; Stratmann, R. E.; Yazyev, O.; Austin, A. J.; Cammi, R.; Pomelli, C.; Ochterski, J. W.; Martin, R. L.; Morokuma, K.; Zakrzewski, V. G.; Voth, G. A.; Salvador, P.; Dannenberg, J. J.; Dapprich, S.; Daniels, A. D.; Farkas, O.; Foresman, J. B.; Ortiz, J. V.; Cioslowski, J.; Fox, D. J. *Gaussian 09*, revision A.01; Gaussian Inc.: Wallingford, CT, 2009.
(20) (a) Bottoni, A.; Frenna, V.; Lanza, C. Z.; Macaluso, G.; Spinelli, D. *J. Phys. Chem. A* **2004**, *108*, 1731−1740. (b) Yamabe, S.; Tsuchida, N.; Miyajima, K. *J. Phys. Chem. A* **2004**, *108*, 2750−2757. (c) Catak, S.; Monard, G.; Aviyente, V.; Ruiz-Lopez, M. F. *J. Phys. Chem. A* **2006**, *110*, 8354−8365.